# Fault-plane reflections as a diagnostic of pressure differences in reservoirs: A case study

Matthew Haney[1], Jon Sheiman[2], Roel Snieder[1], Steve Naruk[2] & Jay Busch[2]
[1] *Center for Wave Phenomena, Colorado School of Mines, Golden, CO 80401*
[2] *Shell International Exploration and Production Inc., Houston, TX 77025*

**ABSTRACT**

Seismic data taken at Blocks 314, 315, 330, and 331 of the South Eugene Island field contain reflections from a major growth fault. Out of a number of possible causes, we find that differences in pore pressure across the fault give rise to the fault-plane reflections. The pressure differences are detectable since pore pressures that exceed the hydrostatic pressure, or overpressures, lower the seismic velocity. Thus, the presence of the reflections point to the fault providing a significant seal. We develop a processing scheme to highlight the fault-plane reflections while simultaneously removing the reflections from the layered structure. Using this processed data set, we extract the amplitude of the fault-plane reflections on the fault-plane itself. The areas of strong reflection amplitude correlate well with the geology and known areas of overpressure.

## INTRODUCTION

The importance of faults as delimiters of compartments in hydrocarbon reservoirs cannot be stressed enough. The role of faults, however, is complicated by their dual nature as both fluid seals and conduits. Classifying a fault as one or the other typically demands extensive knowledge of a basin's geologic history, core samples, and well logs. Only recently have geophysicists begun to incorporate conventional seismic data into the evaluation of fluid pressure near faults (Dutta, 2002a; Huffman, 2002). The method relies on seismic waves detecting the presence of pressure changes in the subsurface (Pennebaker, 1968; Reynolds, 1970), and, when successful, manages to predict regions of overpressure that affect drilling operations.

Evidence of faults can often be seen on migrated seismic data. Automated fault identification algorithms avoid the tedious picking of faults in 3D volumes of seismic data (Townsend *et. al*, 1998). According to Sheriff (1984), the imprints of faults on seismic data are: "(a) abrupt termination of events, (b) diffractions, (c) changes in dip, (d) distortions of dips seen through the fault, (e) deterioration of data beneath the fault producing a shadow zone, (f) changes in the pattern of events across the fault, and (g) occasionally a reflection from the fault plane." Items (a), (c), and (f) provide indirect evidence of faults and form the basis of automated fault identification. Problems with how time migration treats lateral velocity variations lead to items (d) and (e). Here, we address the last point; namely, what are the occasional fault-plane reflections telling us about the nature of the fault itself?

Several fault-zone models describe different aspects of the seismic properties of a fault. One possibility is that the fault is a linear-slip interface (Worthington and Hudson, 2000; Coates and Schoenberg, 1995). Physically, this means that the fault is a zone of low shear modulus. Another model takes into account that the fault may be a barrier to lateral fluid flow. A high shale content in the fault gouge causes fluid pressures to build up on one side of the fault. As a result, the adjacent sediments are undercompacted, and subsequently have lower velocities (Dutta, 1997). Because of throw across the fault, lithological (sand/shale) contacts across a fault can also contribute to reflections from the fault-plane (Sheriff, 1984; Yielding *et. al*, 1991). A main difference in these models is that reflection from a low-shear zone acts as a high-pass filter; in essence, the fault zone is a thin bed. The magnitude of the reflection in this case depends on the seismic properties and thickness of the zone. Pore pressure and lithologic differences across a fault act as traditional seismic interfaces that preserve frequency in the reflection process. A true fault zone could be a combination of two or more of these models.

Here, we show that, at the South Eugene Island field, fault-plane reflections from a major growth fault,

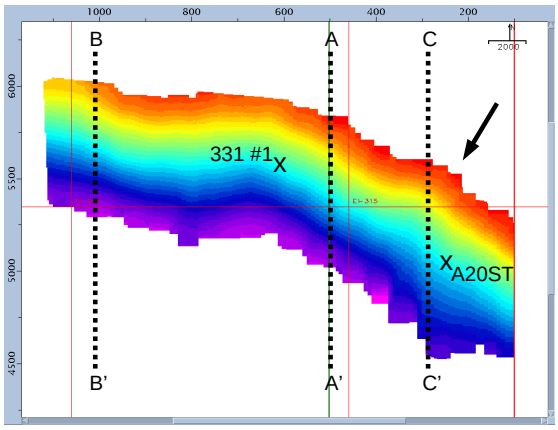


**Figure 1.** Map view of the two-way reflection time from the A-fault. The arrow points in the downdip direction. Two wells are shown by an X where they intersect the fault-plane. The locations of three seismic lines used in other figures are also shown as dashed lines.

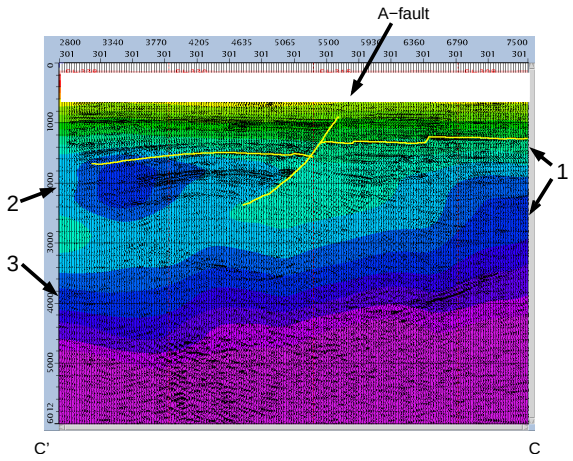


**Figure 2.** Interval velocities along the C-C′ line at the South Eugene Island field obtained via a smoothed Dix-type inversion. The velocity increases monotonically with depth at marker '1', but experiences a decrease between markers '2' and '3'. The decrease in velocity with depth indicates that overpressures are present. The general trend of the high velocity pocket at marker '2' correlates with the A-fault.

known as the A-fault, arise from pore pressure differences across the fault. We focus on this fault since previous studies (Losh *et al.*, 1999) suggest that it serves as a significant barrier to lateral fluid movement. The strength of the fault-plane reflections varies along strike and dip of the A-fault. We make the correlation between areas of fault-plane reflections and areas of strong pressure gradients based on existing well information and known zones of overpressure. No evidence yet suggests that the fault-plane reflections originate from low-shear zones or lithologic contacts.

## OVERPRESSURE AT SOUTH EUGENE ISLAND

Growth faults, or syndepositional normal faults, divide the Pliocene-Pleistocene sediments at South Eugene Island into several compartments. Depending on whether or not the faults are significant barriers to fluid flow, the individual compartments can be overpressured. For instance, Losh *et al.* (1999) report an increase of more than 780 psi in pore pressure over a distance of 18 m while drilling through the A-fault in Block 330 of the South Eugene Island field.

A contour plot of the two-way reflection time from the A-fault is shown in map view in Fig. 1. The arrow in Fig. 1 points in the down-dip direction that makes an angle of approximately 50° with the horizontal. The A20ST well, where Losh *et al.* observed a large pore pressure jump, intersects the fault on the lower right.

Several mechanisms effectively cause anomalously high pore pressures in the subsurface (Dutta, 1997). In the Gulf of Mexico, overpressure commonly results from dipping sands being bounded above and below by shales. The relatively high permeability of the sands allows fluid pressures from depth to move into high points of subsurface structure. Termed unloading, this mechanism results in a seismic velocity decrease due to undercompaction of the sediments. More specifically, the high pore pressure causes a decrease in the vertical effective stress and, as a result, a decrease in the area of grain-to-grain contacts.

We have identified anomalous decreases in velocity from a smoothed Dix-type inversion on the South Eugene Island data. Line C-C′ (see Fig. 1) from this velocity cube is displayed in Fig. 2. The velocity at marker '1' monotonically increases with depth. This represents the velocity variation resulting from the normal compaction trend. On the left side of this plot, between markers '2' and '3', a noticeable decrease in velocity occurs with increasing depth. Experience has shown that, in the Gulf of Mexico, such a decrease in velocity with depth is due to high pore pressures rather than lithology (Dutta, 1997). The spatial pattern of the relatively higher velocity pocket at '2' corresponds to the trend of the A-fault, providing evidence from the seismic data that the overpressures are related to the A-fault.

Zones of overpressure can be monitored while drilling from the rate of penetration of the drill bit into the formation (Jordan and Shirley, 1966). Such a method suffices for detecting the gradual build up of overpressure above a moderately sealing shale. By moderately sealing, we mean that the pressure front has, over geologic time, diffused somewhat through the shale. Any sort of overpressure prediction while drilling should fail when a highly overpressured zone is quickly and unexpectedly encountered. This has motivated the

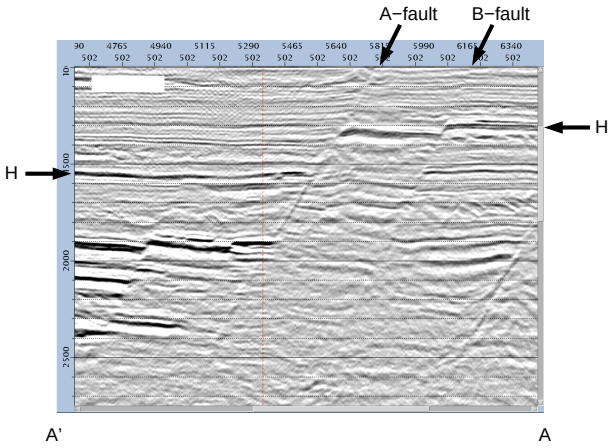


**Figure 3.** A typical fault-plane reflection from the A-fault along the A-A′ line. Shown is the post-stack time-migrated image. The H-sand is marked to show the amount of throw across the fault.

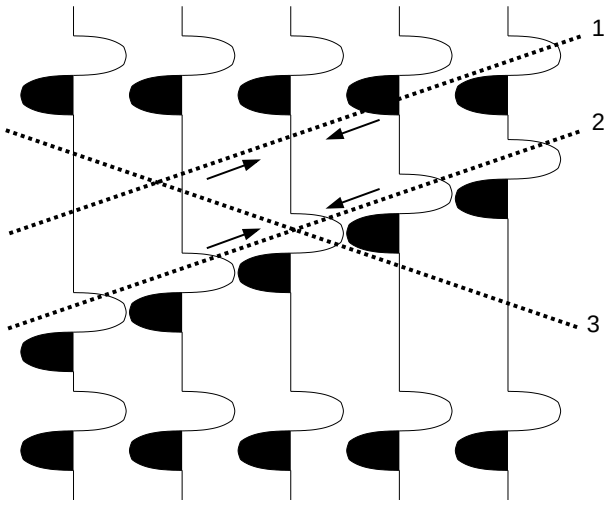


**Figure 4.** The slant stack technique used to accentuate the fault-plane reflections. Stack '1' is zero since it intersects the upper horizontal reflection at an angle. The fault-plane reflection coherently adds into stack '2'. We also stacked in the opposite direction '3' to capture any antithetic faults.

development of pre-drill pore pressure prediction from seismic data.

For a smooth increase in fluid pressure across a moderate seal, the velocity decreases gradually, and a transmitted wave passes through the overpressured region with almost no reflection. However, the most dangerous instances of overpressure occur over distances less than a typical seismic wavelength ($\sim$ 200 m), and therefore, quick onsets of high fluid pressure across a sealing fault give rise to strongly reflected waves. By mapping out the amplitude of fault-plane reflections on the fault-plane itself, areas of sharp increase in pore pressure across the fault, as described in Losh *et al.*, should stand out.

## ISOLATING FAULT-PLANE REFLECTIONS

Even at their strongest, the fault-plane reflections at South Eugene Island are less prominent than the layer reflections. This may be due to either small reflectivity at the fault or the deterioration of the imaging procedure (Kirchhoff) for steep dips. As a result, the fault image contains "noise" from the horizontal layers terminating at the fault. We employ a simple slant stack along the fault to effectively remove the layers while at the same time accentuating the reflection from the fault plane.

Displayed in Fig. 3 is a post-stack time migrated section along the A-A′ line (see Fig. 1). Several growth faults stand out in this image. A particularly strong fault-plane reflection cuts through the center of Fig. 3 - this is the A-fault. To the right, another fault (the B-fault) can be made out from the mismatch of adjacent layers; however, the B-fault does not give rise to a reflection. This is likely because the throw on the A-fault is greater than that on the B-fault. We have highlighted the H-sand as an indicator of the throw on these two faults. The greater the throw on a fault, the more developed its gouge, and, therefore, the more likely it is to be a barrier for lateral fluid flow.

To bring the fault-plane reflections out, we designed an adaptive local slant stack routine. Pictured in Fig. 4 is the basic procedure. Along each trace, we scan over a small angular window for the maximum coherence direction. The range of angles is selected to correspond to the dip of the fault. We then construct the slant stacks by summing over the five adjacent traces. In Fig. 4, we show two layer reflections with no dip and a dipping fault-plane reflection. Slant stack '1' does not lie in the fault-plane and the contributions from the upper layer cancel. In contrast, '2' lies in the fault plane and the fault-plane reflection coherently stacks. Since faults in an extensional regime typically have antithetic counterparts, we also stack in the opposite direction '3'.

A slant stack is shown as a wiggle-plot in Fig. 5 with the migrated image of Fig. 3 in the background. The horizontal layers effectively cancel in the stack, leaving the fault-plane reflections to stand out. Both the amplitude and phase of the fault-plane reflection from the A-fault vary along the fault. The phase seems to change at points where sandstones encounter the fault. For instance, moving up the fault-plane from the bottom, the wavelet changes shape and grows stronger as it moves past the JD-sand. It then vanishes between the downthrown and upthrown segments of the H-sand, only to continue again above the upthrown H-sand.

We cannot make quantitative use of the phase yet since the absolute phase of the reflections may be contaminated with stacking and migration errors. Future

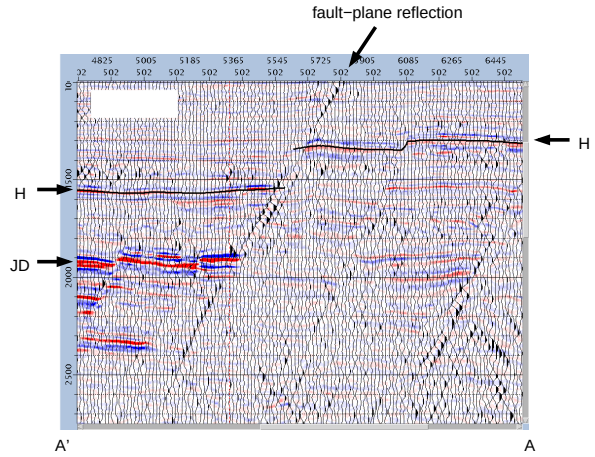


**Figure 5.** Overlay of the time-migrated seismic section from Fig. 1 with the wiggle-trace slant stack. The fault-plane reflection becomes clearer in the slant stack.

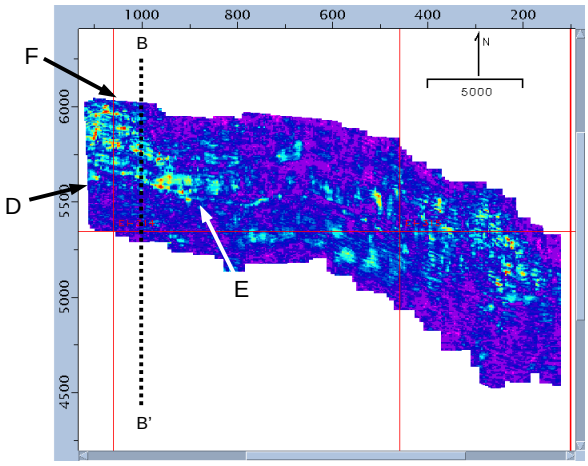


**Figure 6.** Reflection amplitude from the A-fault as a function of position on the fault-plane. The view is the same as in Fig. 1. Stronger amplitudes show up as lighter colors. Points D, E, and F delineate a triangle of higher amplitude on the upper left. Line $\overline{\text{DE}}$ is the intersection of the overpressured JD-sand with the A-fault. Line $\overline{\text{EF}}$ marks the convergence of the A-fault with an antithetic fault. The dashed line B-B′ is a seismic section shown in Fig. 7.

numerical work will attempt to get a handle on this error. For example, the phase would be an excellent indicator of high fluid pressures inside a fault-zone. High fluid pressure in the A-fault has been reported by Losh *et al.* (1999) and leads to small shear velocities in the fault. Since scattering from such a linear slip interface is frequency dependent, the phase of the reflected wavelet could change. Though we cannot trust the absolute phase, we interpret the relative phase changes along the fault to be related to occurrences of the sands.

We extended the above procedure to 3D to gain a more extensive picture of the variations in fault-plane reflections. By breaking up the 3D seismic data volume into successive 2D planes, we could perform the slant stacking on each plane individually. The slant-stacked lines were then reassembled into a 3D data volume.

## CORRELATION OF FAULT-PLANE REFLECTIONS WITH REGIONS OF OVERPRESSURE

The attributes of the slant-stacked 3D seismic data on the A-fault contain information about the fault seal. Using Shell's Rosebud seismic attributes software, we extracted the maximum amplitude along the picked fault-plane (Fig. 1) within a small time gate. The reflection amplitudes are displayed in map view on the fault plane in Fig. 6. The view in this figure is identical to the view in Fig. 1. Higher amplitudes, shown as lighter colors in Fig. 6, come and go on the fault plane. We save discussing the details of the reflections except in a triangle in the upper left portion of the fault, labeled as points D, E, and F in Fig. 6.

The triangle DEF forms the most strikingly coherent feature on the amplitude map and its two sides $\overline{\text{DE}}$ and $\overline{\text{EF}}$ have geologic meaning. The time-migrated image and the slant stack along the B-B′ line (see Fig. 6) are shown in Fig. 7. The intersection of $\overline{\text{DE}}$ with the B-B′ line corresponds to the meeting of the A-fault and the JD-sand. The lack of strong amplitudes south of $\overline{\text{DE}}$ in Fig. 6 means that the A-fault does not reflect below the JD horizon. This is likely because the JD-sand is itself overpressured. Stump *et al.* (1998) have observed that at well 331 #1 (see Fig. 1) the JD-sand marks the onset of overpressure in the sedimentary column. Essentially, beneath the JD horizon, both sides of the A-fault are overpressured and, hence, no reflection occurs from the fault-plane. Below the JD-sand, the smaller fault to the left of the A-fault (Fig. 7) is reflecting, suggesting that this fault forms a seal. Line $\overline{\text{EF}}$ marks the intersection of the A-fault with the antithetic fault shown in Fig. 7. The lack of strong amplitudes north of $\overline{\text{EF}}$ in Fig. 6 means that the A-fault does not reflect above the top of the wedge formed by it and the antithetic fault. Since the antithetic fault is reflecting, this suggests that the seal transfers from the A-fault to the antithetic fault at the top of the wedge. The presence of lower velocities, consistent with higher pore pressures, on the upthrown side of the A-fault is supported by the results of the Dix-type velocity inversion (Fig. 2).

## CONCLUSIONS

At the South Eugene Island field, observed fault-plane reflections from the A-fault arise due to pressure differences across the fault. By applying a technique to accentuate the fault-plane reflections, we are able to

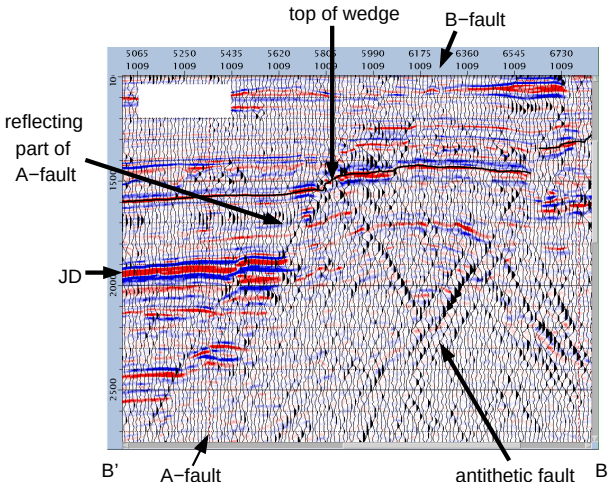


**Figure 7.** An overlay of the time-migrated seismic section along line B-B′ with the wiggle-trace slant stack. An antithetic fault exists at this location. The reflecting part of the A-fault corresponds to the part of it between the JD-sand and the top of the wedge formed by the antithetic fault.

map out the reflection amplitudes on the fault plane. The spatial distribution of the reflections has a geologic meaning and shows which part of the fault-plane is acting as a seal. Future work will focus on other faults in the South Eugene Island field and attempt to get quantitative estimates of fault-zone properties from the fault-plane reflections.

## ACKNOWLEDGMENTS

The authors wish to thank Shell International Exploration and Production for funding this research.

## REFERENCES

Coates, R. T. and Schoenberg, M. 1995. Finite-difference modeling of faults and fractures. *Geophysics*, **60**, *1514*.

Dutta, N. C. 1997. Pressure prediction from seismic data: implications for seal distribution and hydrocarbon exploration and exploitation in the deepwater Gulf of Mexico, in: *Hydrocarbon Seals: Importance for Exploration and Production*, eds. P. Moeller-Pederson and A. G. Koestler, Elsevier, Singapore.

Dutta, N. C. 2002a. Deepwater geohazard prediction using prestack inversion of large offset $P$-wave data and rock model. *The Leading Edge*, **21**, *193*.

Dutta, N. C. 2002b. Geopressure prediction using seismic data: Current status and the road ahead. *Geophysics*, **67**, *2012*.

Huffman, A. R. 2002. The future of pore-pressure prediction using geophysical methods. *The Leading Edge*, **21**, *199*.

Jordan, J. R. and Shirley, O. J. 1966. Application of Drilling Performance Data to Overpressure Detection. *Journal of Petroleum Technology*, **1387**, *18*.

Losh, S., Eglinton, L., Schoell, M., and Wood, J. 1999. Vertical and Lateral Fluid Flow Related to a Large Growth Fault, South Eugene Island Block 330 Field, Offshore Louisiana. *AAPG Bulletin*, **83**, *244*.

Pennebaker, E. S. 1968. Seismic data indicate depth, magnitude of abnormal pressures. *World Oil*, **166**, *73*.

Reynolds, E. B. 1970. Predicting overpressured zones with seismic data. *World Oil*, **171**, *78*.

Sheriff, R. E. 1984. *Encyclopedic Dictionary of Exploration Geophysics*, SEG.

Stump, B., Flemings, P., Finkbeiner, T., and Zoback, M. 1998. Pressure differences between overpressured and bounding shales of the Eugene Island 330 field (offshore Louisiana, USA) with implications for fluid flow induced by sediment loading, in: *Overpressures in petroleum exploration: workshop proceedings*, eds. A. Mitchell and D. Grauls, Elf Exploration Production Memoir 22.

Townsend, C., Firth, I. R., Westerman, R., Kirkevollen, L., Harde, M., and Andersen, T. 1998. Small seismic-scale fault identification and mapping, in: *Faulting, Fault Sealing and Fluid Flow in Hydrocarbon Reservoirs*, eds. G. Jones, Q. J. Fisher, and R. J. Knipe, Geological Society Special Publication No. 147.

Worthington, M. H., and Hudson, J. A., 2000. Fault properties from seismic $Q$, *GJI*, **143**, *937*.

Yielding, G., Badley, M. E., and Freeman, B. 1991. Seismic reflections from normal faults in the northern North Sea, in: *The Geometry of Normal Faults*, eds. A. M. Roberts, G. Yielding, and B. Freeman, Geological Society Special Publication No. 56.